ELSEVIER

Solid State Ionics 145 (2001) 429–435

SOLID STATE IONICS

www.elsevier.com/locate/ssi

The combined neutron scattering and first-principles study of solid state protonic conductors

T. Yildirim [a,*], B. Reisner [b], T.J. Udovic [a], D.A. Neumann [a]

[a] *NIST Center for Neutron Research, National Institute of Standards and Technology, Room E112, Building 235, 100 Bureau Dr., Gaithersburg, MD 20899-8562, USA*

[b] *Department of Chemistry, James Madison University, Harrisonburg, VA 22807, USA*

Received 23 October 2000; received in revised form 23 February 2001; accepted 6 April 2001

Abstract

The need for more efficient batteries and fuel cells to be used for vehicle propulsion, photovoltaic energy storage, and self-contained power sources has led to increased effort in the development of improved materials with high proton conductivity. In this paper, we outline the utility of neutron scattering methods in conjunction with first-principles total-energy calculations for characterizing the structure and proton dynamics in such materials, namely, $SrCe_{1-x}Sc_xO_{3-\delta}H_y$, $Ba_2In_2O_{5+\delta}H_{2\delta}$ and $RbHSO_4$.

Keywords: Proton conductors; Neutron scattering; First-principles calculations; Density functional; Strontium cerate; $Ba_2In_2O_5$; $RbHSO_4$

1. Introduction

Materials with high protonic conductivity are candidates for electrolytes in sensors, batteries, and solid oxide fuel cells [1]. The typical protonic conductors developed a couple of decades ago were mainly acidic or hydrous inorganic compounds [1,2]. Later, entirely different classes of materials gained increasing recognition as potential proton conductors including polymers, oxide ceramics, and intercalation compounds [2]. This has led to increased interest in experimental and computational techniques that can provide detailed atomistic information about proton incorporation and dynamics in these systems. In this respect, neutron scattering [3] is a useful probe of the proton dynamics and thus the proton conductivity mechanism in these materials because of the relatively large neutron scattering cross-sections for hydrogen. Furthermore, thermal neutrons have wavelengths and energies that are comparable with interatomic distances and typical solid state excitations, respectively. Thus, neutrons may be used to investigate atomic structures, probe dynamical phenomena, and determine the spatial character of an excitation in a manner unmatched by other spectroscopic probes [3,4].

The power of neutron scattering as a probe of proton dynamics can be further enhanced by combining it with the predictive power of first-principles density functional calculations [5]. With today's available computer power, it is now possible to predict structural and dynamical properties of many new materials using first-principles calculations based on

* Corresponding author. Tel.: +1-301-975-6228; fax: +1-301-921-9847.

E-mail address: taner@nist.gov (T. Yildirim).

URL: http://www.ncnr.nist.gov/staff/taner.

0167-2738/01/$ - see front matter
PII: S0167-2738(01)00940-7

density functional theory (DFT) within the local density approximation (LDA). For example, by comparing the measured neutron inelastic spectrum and calculations, we can unambiguously identify the hydrogen modes observed in the spectrum [5].

In this paper, we review the utility of neutron scattering methods in conjunction with first-principles calculations for characterizing the nature of the proton–lattice interactions and associated proton dynamics. We hope that such information will help foster the development of new solid state protonic conductors (SSPCs) with higher proton conductivity. In the next section, we will briefly describe different neutron techniques and then present some data and calculations on three classes of protonic conductors, namely, $SrCe_{1-x}M_xH_yO_{3-\delta}$ perovskites (where M = Sc, Nd and Ho), Brownmillerite-structured oxide-based protonic conductors (i.e. $Ba_2In_2O_5$), and alkali hydrogen sulfate $RbHSO_4$.

2. Neutron scattering techniques and calculations

We have used a variety of neutron scattering techniques at the NIST Center for Neutron Research (NCNR) to investigate proton dynamics in solid state proton conductors (SSPCs). All the neutron measurements reported here were performed using the beam lines at the NCNR [6,7]. The first-principles total-energy and force calculations have been performed using the pseudopotential planewave code CASTEP [8]. The results have been obtained within the generalized gradient approximation (GGA) using a 400-eV cutoff energy, *k*-point sampling with *k*-spacing of 0.07 $Å^{-1}$, and ultrasoft pseudopotentials. All the energies converged within 0.5 meV/atom. The zone-center phonons (i.e. $Q = 0$) were obtained by forming the dynamical matrix using the direct-force method with finite displacement [5].

2.1. Neutron powder diffraction

Similar to X-ray diffraction, neutron powder diffraction (NPD) is invaluable for determining the structure and purity of condensed phase materials [6] such as the SSPCs via Rietveld refinement. However, unlike X-rays, structures obtained from neutron diffraction are usually more accurate because neutrons are scattered directly from the nuclei rather than the atomic electrons. In addition, elements such as H and Li, which are almost invisible to X-rays, can be probed by neutrons. Hence, if the protons (or more appropriately the deuterons for NPD) in the SSPCs are located in structurally unique crystallographic positions, then NPD can also provide information about their location in the lattice.

In order to demonstrate the power of NPD, we present here our preliminary in situ structural study of hydration phases of the Brownmillerite-type oxide $Ba_2In_2O_5$. These materials have been attracting attention recently as possible fast proton conductors for use in solid oxide fuel cells [9–11]. The structure of the $A_2B_2O_5$ compounds is derived from the ABO_3 perovskite structure in which the tetravalent B cations have been completely substituted by cations one less in valency. To maintain charge balance, one-sixth of the anions are removed, and therefore, the Brownmillerite structure has a high concentration of oxygen vacancies. X-ray diffraction measurements indicate that these vacancies are trapped in ordered parallel rows, inhibiting rapid oxygen-anion conduction at moderate temperatures [10,11]. This suggests that hydrated $A_2B_2O_5$ may exhibit pure protonic conduction. However, little is currently known concerning the hydration process and the proton locations in these systems.

Fig. 1 shows the NPD profiles of a $Ba_2In_2O_5$ sample in controlled humid (D_2O) air as a function of temperature. From this study, we clearly identified at least two distinct hydration phases of the $Ba_2In_2O_5$–xD_2O system. At temperatures above 623 K, we observe only the undoped $Ba_2In_2O_5$ phase. Rietveld refinement of this phase (shown in Fig. 1) gave the precise atomic positions and confirmed the structure which was reported from a previous X-ray study [11]. At around 573 K, we observed a new phase (middle curve in Fig. 1). Similarity of the powder pattern of this phase to the undoped one indicates that the structure is only slightly perturbed upon light hydration. However, the Bragg peak at low angle (denoted by '+' in Fig. 1) indicates that the unit cell along the *c*-axis may be doubled. This suggested that one of the two interstitial sites available in $Ba_2In_2O_5$ along the *c*-axis was occupied in an ordered manner. Upon lowering the temperature further, this phase disappears and a fully hydrated

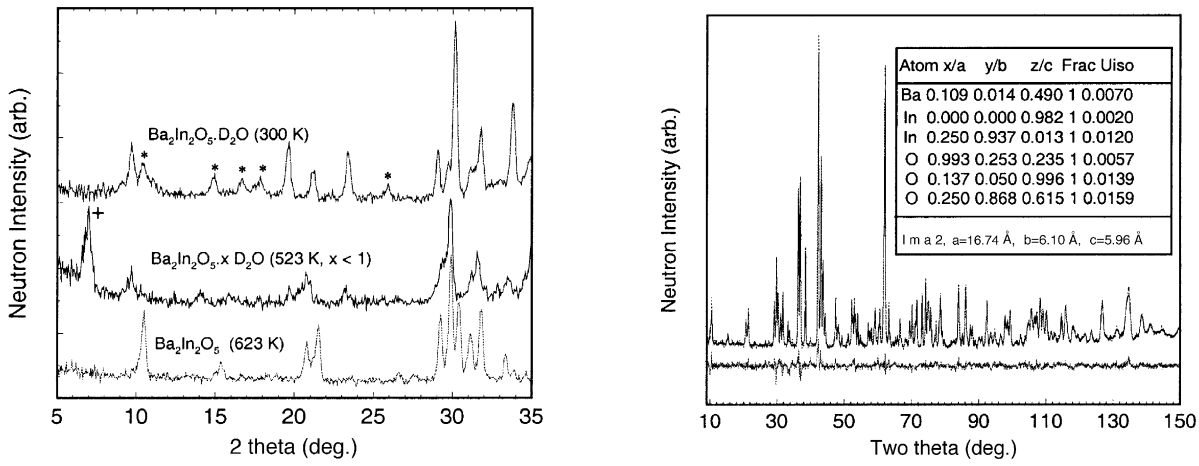

Fig. 1. Left: NPD pattern of $Ba_2In_2O_5$–xD_2O at various temperatures in humid air. Right: NPD pattern and corresponding structural fit for the undoped phase $Ba_2In_2O_5$ at room temperature. The bottom pattern is the difference plot. The inset shows the refinement results for the structural parameters.

$Ba_2In_2O_5$ phase is formed as shown in the top panel of Fig. 1. Most of the peak positions and intensities of this phase can be explained from a simple ABO_3 perovskite structure as initially proposed from the X-ray study [11]. A Rietveld refinement based on the X-ray model is shown in Fig. 2. However, as shown in Fig. 1 by '*', not all the Bragg peak positions can be accounted for by this X-ray structure. Interestingly, these new peaks are at the positions expected from a new cell with the lattice constant doubled in the *a*- and *b*-directions. Therefore, present measurements clearly indicate that the structure of the fully hydrated $Ba_2In_2O_5$ phase is not the one reported from the X-ray diffraction study [11]. Rather, it is a superstructure, and because protons are invisible to X-rays, these superstructure peaks must arise from

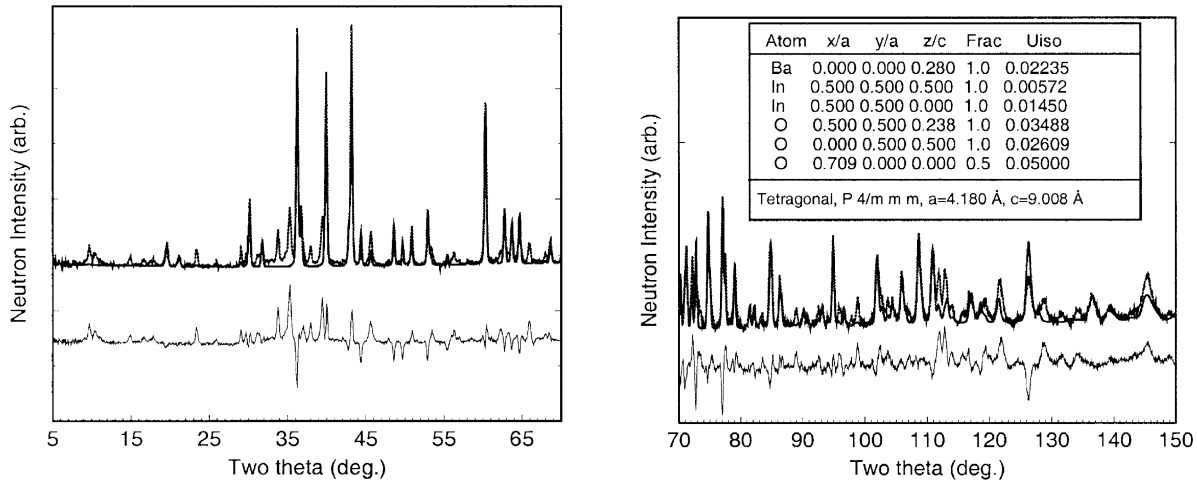

Fig. 2. The low (left) and high (right) angle portions of the neutron powder diffraction profile (dotted line), the fit (solid line), and the difference plot (bottom line) for $Ba_2In_2O_6D_2$ using the X-ray model without D [11].

proton ordering in the solid. We are currently performing Rietveld refinements in order to pinpoint the proton locations and the possible sublattice ordering of the protons [12]. This effort promises to yield a detailed understanding of the structure of these systems.

2.2. Inelastic neutron scattering (INS)

Inelastic neutron scattering (INS) [7] provides a means of probing the bonding potentials experienced by the protons in the lattice. Since the protons bind with oxygen from the perovskite lattice to form OH^- species, dopant-related perturbations to the vibrational energies of these species would be confirmation of the trapping effects of the dopant cations. This was indeed seen to be the case from the INS measurements of $SrCe_{0.95}M_{0.05}H_xO_{3-\delta}$ (M = Sc, Ho and Nd) [13] illustrated in Fig. 3(left), where the OH^- bending-mode energy (located in the region above 90 meV) occurs at around 115 and 105 meV in the Sc- and Ho-doped oxides, respectively. The corresponding mode in the spectrum of the Nd-doped sample seems to be superimposed on the mode at 80 meV. Therefore, the bending-mode energy could be correlated with the size of the dopant cation, generally increasing for smaller cations. Such a dependence reflects changes in the lattice potential experienced by the protons, which ultimately affects the proton jump rates between potential wells in the lattice.

In order to identify the features observed in the INS spectrum shown in Fig. 3, we performed lattice dynamics calculations on a $\sqrt{2} \times \sqrt{2} \times 1$ supercell of $SrCeO_3$. Replacing one Ce in this supercell by (Sc + H) yielded a cell formula $Sr_8Ce_7ScHO_{24}$, which is close to the experimental system. In $Sr_8Ce_7ScHO_{24}$, protons can be either at the 'undoped' (U) or 'doped' (D) sites. We have performed calculations for both cases, and the optimized structures are shown in Fig. 3(middle). We found that the doped site has a much lower energy (−1.13 eV) than the undoped site. This is primarily because the proton prefers to be closer to the Sc cation, which has a charge of +3 compared to +4 for Zr. Even though the MO_6 octahedra are quite rigid, the distortions due to the presence of the proton at these sites are quite large, giving rise to very different vibrational spectra. In both cases, the proton forms an OH bond with bond lengths of 0.976 and 1.001 Å at the U and D sites, respectively. While these bond lengths are quite similar, the distance between the proton and the other nearest-neighbor oxygen is quite different. This is undoubtedly due to the Coulomb interaction between the proton and the M cation.

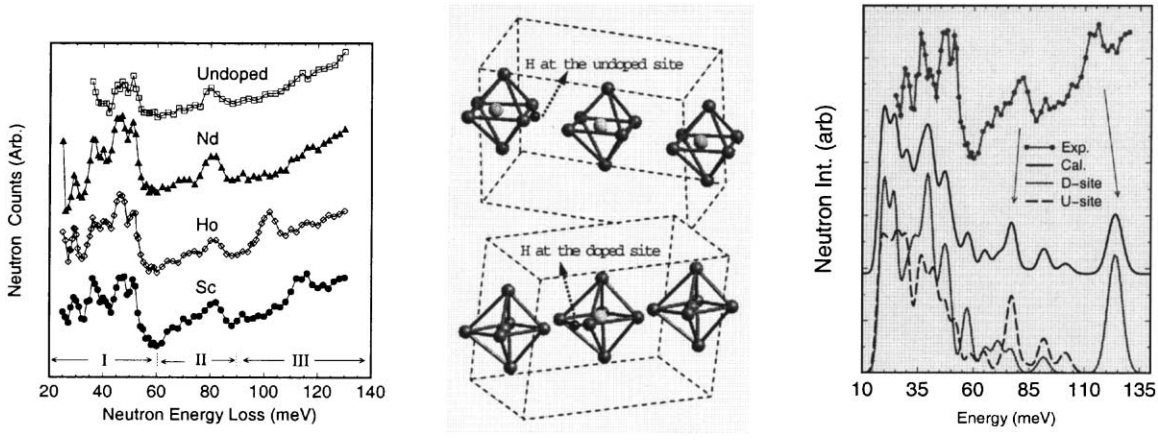

Fig. 3. Left: INS spectra for $SrCe_{1-x}M_xH_yO_{3+\delta}$ samples, revealing three well-defined vibrational bands in the energy ranges 20–60, 60–90, and 100–140 meV. Middle: Optimized structures when the proton is trapped at the undoped site (top) and at the doped site (bottom). For clarity, not all atoms are shown. Right: Comparison of the neutron vibrational spectra of $SrCe_{1-x}Sc_xH_xO_3$ (top) and calculated. Dashed and dotted lines shown at the bottom are the contributions from the H–MO_6 clusters, where M = Ce (U site) and M = Sc (D site), respectively.

To investigate this further, we performed 'embedded cluster' calculations in which the vibrational spectrum of only the H–MO_6 cluster is calculated while all other atoms are kept at their equilibrium positions. The two tangential OH^- bending modes are found to be quite different depending on whether the proton is at the Ce or Sc site. If it is at the Sc site, the lowest tangential mode is found at 122.9 meV. However, if it is at the Ce site, the mode is much softer at around 88.5 meV. Interestingly, in the INS spectrum (top curve in Fig. 3(right)), we observe features at these energies upon proton addition. The total spectrum (superposition of the spectra from H–CeO_6 and H–ScO_6 clusters) as well as the contributions from individual clusters are shown in Fig. 3. The similarity between experiment and calculation suggests that the mode observed near 120 meV is due to protons trapped at the Sc sites, while some portions of the peak near 80 meV are due to protons at the undoped sites. In order to study this more quantitatively, we are currently extending our calculations to different dopant types.

To further probe the hydration process and OH formation in SSPCs, we initiated INS measurements of the $Ba_2In_2O_5$–xH_2O and $Ba_2In_2O_5$–xD_2O systems. The left panel in Fig. 4 shows our preliminary results for the vibrational spectrum of $Ba_2In_2O_5$–xH_2O with $x \approx 0.5$ and $x \approx 1$ and $Ba_2In_2O_5$–D_2O. Comparing the spectra of $Ba_2In_2O_5$–xD_2O and $Ba_2In_2O_5$–xH_2O indicates that modes above 85 meV scale with the square root of proton mass. This is a clear demonstration that these modes are due primarily to hydrogen vibrations. The similarity of the spectrum above 85 meV for samples with $x \approx 0.5$ and $x \approx 1$ indicates that the local environment of protons in the lightly doped and the fully doped phases are quite similar. However, in the fully hydrated phase, we observe many features around 35–70 meV, which are most likely coupled oxygen–hydrogen modes. Absence of these modes in the $x \approx 0.5$ sample indicates that the protons in this phase have only a slight effect on the oxygen ions. We are also carrying out first-principles calculations in order to probe the bonding potentials experienced by the residual protons. The right panel shows the INS spectrum of the $x \approx 0.5$ sample with a better resolution and a simple first-principles model calculation. Since we do not know the actual position of the

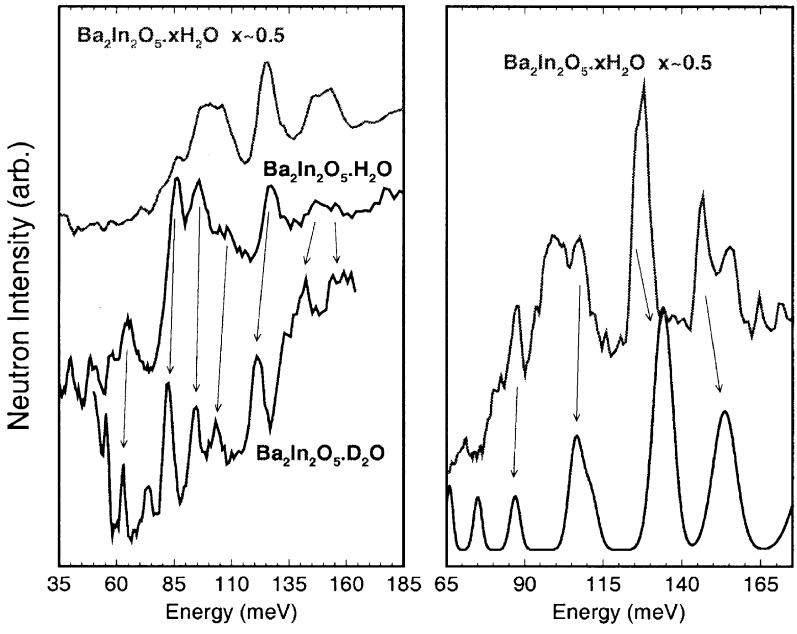

Fig. 4. Left: INS spectrum of $Ba_2In_2O_5$–xH_2O. The energy axis of $Ba_2In_2O_5$–D_2O is scaled by $\sqrt{2}$ to compare the two spectra. Right: A higher resolution INS spectrum of $Ba_2In_2O_5$–xH_2O and a model calculation (bottom).

protons in the structure yet, the calculations are carried out assuming an InO_6–H octahedral cluster in the Brownmillerite structure. The moderate agreement between the data and this preliminary calculation further confirms OH formation and existence of InO_6–H octahedral clusters in the system.

The final example concerns the hydrogen dynamics in $RbHSO_4$ [14–18]. Fig. 5 summarizes the temperature-dependent INS measurements. First-principles studies are underway to interpret the experimental data [14]. The INS spectrum shows a very sharp peak around 99.7 meV, which is also typical for the M = Cs sample. An unusual temperature dependence is observed for the 99.7 and 83.3 meV peaks. Both peak intensities decrease very rapidly with increasing temperature and almost disappear at temperatures as low as 200 K. As shown in Fig. 5, the modes near 100 and 83 meV decrease and increase in energy (about 2–4 meV) with increasing temperature, respectively. Near 200 K, these two modes appear to collapse to form a broad background around 95 meV. This suggests that there is significant proton motion even at this low temperature. We are currently studying this further by NPD measurements on deuturated samples to see if we can monitor any significant changes in the structure at these temperatures. We believe that these modes are related to the hydrogen motions between two oxygen ions, which are bounded by strong hydrogen bonds.

3. Conclusion

In summary, we present several neutron scattering measurements in conjunction with first-principles calculations to demonstrate the potential for these combined techniques to provide a unique means of characterizing the proton dynamics in the SSPCs. Briefly, INS measurements and calculations in doped perovskites indicated that hydrogen ions are initially trapped randomly at the doped and undoped sites. However, the trapping energy is lower at the doped site (i.e. M^{+3}) than at the undoped site (i.e. M^{+4}) due to Coulomb interactions. In situ NPD measurements of $Ba_2In_2O_5$ clearly show two new phases

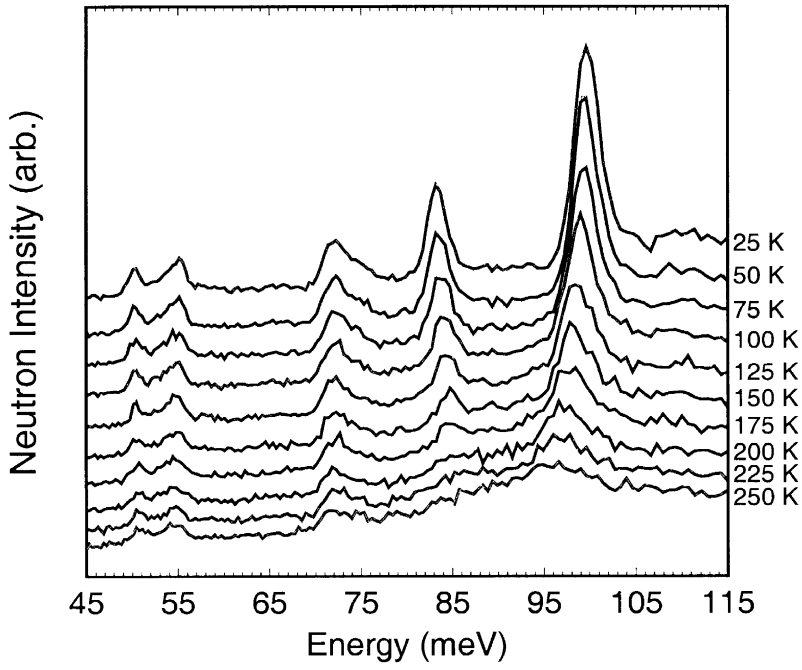

Fig. 5. INS spectrum of $RbHSO_4$ as a function of temperature. Intensities of the proton modes near 83.3 and 100 meV rapidly decrease with increasing temperature.

with hydration. In the lightly doped regime, we observed very low angle reflections, indicating a possible doubling of the cell along the *c*-axis. In the fully hydrated phase, NPD clearly shows that the correct structure is a supercell doubled along the *a*- and *b*-axes of the ABO_3 perovskite unit cell. INS measurements in conjunction with calculations clearly indicate the formation of OH in $Ba_2In_2O_5$ similar to that observed in perovskites. Finally, temperature-dependent INS measurements of $RbHSO_4$ indicate a very unusual decrease in the intensity of the proton modes near 100 and 83 meV, suggesting that very large amplitude proton motions are present at temperatures as low as 100 K.

Acknowledgements

We would like to acknowledge many useful discussions with S. Haile and C. Chisolm. We also acknowledge the support of the National Institute of Standards and Technology, US Department of Commerce, in providing the neutron facilities used in this work.

References

[1] K. Kordesch, G. Simader, Fuel Cells and Their Applications, VCH Publishers, New York, 1996.
[2] P. Colomban (Ed.), Proton Conductors: Solids, Membranes, and Gels—Materials and Devices, Cambridge Univ. Press, 1992.
[3] S. Lovesey, Theory of Neutron Scattering from Condensed Matter, 3rd edn., Oxford Univ. Press, New York, 1987.
[4] D.J. Jones, J. Roziere, Solid State Ionics 61 (1993) 13; A.V. Belushkin, Solid State Ionics 125 (1991) 61.
[5] T. Yildirim, Chem. Phys. 261 (2000) 205.
[6] J.R.D. Copley, D.A. Neumann, W.A. Kamitakahara, Can. J. Phys. 73 (1995) 763.
[7] D.A. Neumann, B. Hammouda, J. Res. Natl. Inst. Stand. Technol. 98 (1993) 89.
[8] M.C. Payne, M.P. Teter, D.C. Arias, J.D. Joannopoulos, Rev. Mod. Phys. 64 (1992) 1045.
[9] G.B. Zhang, D.M. Smyth, Solid State Ionics 82 (1995) 153.
[10] T. Schober, J. Friedrich, F. Krug, Solid State Ionics 99 (1997) 9.
[11] W. Fischer, G. Reck, T. Schober, Solid State Ionics 116 (1999) 211.
[12] T. Yildirim, B. Reisner, D.A. Neumann, Solid State Ionics (2000) (in preparation).
[13] C. Karmonik, T. Yildirim, T.J. Udovic, J.J. Rush, R. Hempelmann, Mater. Res. Soc. Symp. Proc. 496 (1998) 199.
[14] T. Yildirim, Z. Chowdhuri, D.A. Neumann, T.J. Udovic, Solid State Ionics (2000) (in preparation).
[15] M. Gargouri, T. Mhiri, A. Daoud, T. Jouini, Phys. Status Solidi 200 (1997) 3.
[16] M. Gargouri, R.B. Hassen, T. Mhirir, A. Daoud, J. Phys.: Condens. Matter 10 (1998) 8235.
[17] M. Gargouri, T. Mhiri, A. Daoud, J.M. Reau, Solid State Ionics 125 (1999) 193.
[18] A.V. Belushkin, C.J. Carlile, L.A. Shuvalov, J. Phys.: Condens. Matter 4 (1992) 389; A.V. Belushkin et al., J. Phys.: Condens. Matter 6 (1994) 5823.